Review Article

Tomoyuki Matsuyama*

Exposure tool control for advanced semiconductor lithography

DOI 10.1515/aot-2015-0026
Received March 24, 2015; accepted June 9, 2015; previously published online July 3, 2015

Abstract: This is a review paper to show how we control exposure tool parameters in order to satisfy patterning performance and productivity requirements for advanced semiconductor lithography. In this paper, we will discuss how we control illumination source shape to satisfy required imaging performance, heat-induced lens aberration during exposure to minimize the aberration impact on imaging, dose and focus control to realize uniform patterning performance across the wafer and patterning position of circuit patterns on different layers. The contents are mainly about current Nikon immersion exposure tools.

Keywords: ArF immersion; microlithography; multiple patterning.

1 Introduction

The trend of increase of the number of components per chip, which had been doubling every 18 months, is called Moore's law [1] because it was originated by Gordon Moore in 1965. The actual number of transistors has been generally following this trend for a long time. To allow this, lithography exposure tools for each generation have been developed, which can transfer enough information to generate the required number of transistors on a chip for each generation or timing by reducing the resolution half pitch *R*. That half pitch is obtained by imaging optics on the exposure tool, defined by the equation below.

$$R = k_1 \frac{\lambda}{NA}, \quad (1)$$

where λ, is wavelength, and k_1 is a constant process factor.

Historically, as shown in the equation, resolution half pitch has been reduced by increasing the numerical aperture (NA) of the imaging optics and by reducing the illumination wavelength. In addition to these, k_1 factor has also been reduced by applying various resolution enhancement techniques, such as oblique angle illumination, phase shift mask, improvement of resist performance, etc. In general, lithography with a small k_1 factor, roughly <0.4, is called low k_1 lithography. Until the k_1 factor reached about 0.4, we may be able to say that this era of history of lithography was a golden age, because we were able to deliver tools with required performance by just upgrading previous generation technologies.

Currently, 1.35 NA ArF (argon fluoride excimer laser light source: wavelength of 193 nm) water immersion lens is used for the latest lithography tool for high-volume manufacturing. Though we were trying to reduce the resolution half pitch by increasing NA and reducing wavelength by applying high refractive index material for the lens element and immersion, NA and wavelength are stuck with the current value due to the lack of such high-index materials. Although extreme ultra violet lithography (EUVL) has been under development, due to extreme ultra violet (EUV) infrastructure issues, ArF immersion lithography may be mainly used for further low k_1 lithography even beyond the optics theoretical limit (k_1=0.25) in conjunction with various pattern-resolution reduction processing techniques such as multiple patterning [2]. Multiple patterning is a technique to enhance resolution by processing.

Figure 1 shows current lithography technology trends for logic, DRAM memory, and NAND memory manufacturing. With the logic device scaling trend toward the 7-nm node, the industry has come to a realization and acceptance of extending ArF immersion lithography in conjunction with pitch splitting litho-etch-litho-etch (LEn: multiple use of combination of lithography patterning and etching process) [3], self-aligned double patterning

***Corresponding author: Tomoyuki Matsuyama,** Nikon Corporation, Kumagaya, Saitama 360-8559, Japan,
e-mail: Tomoyuki.Matsuyama@nikonoa.net; www.nikon.co.jp

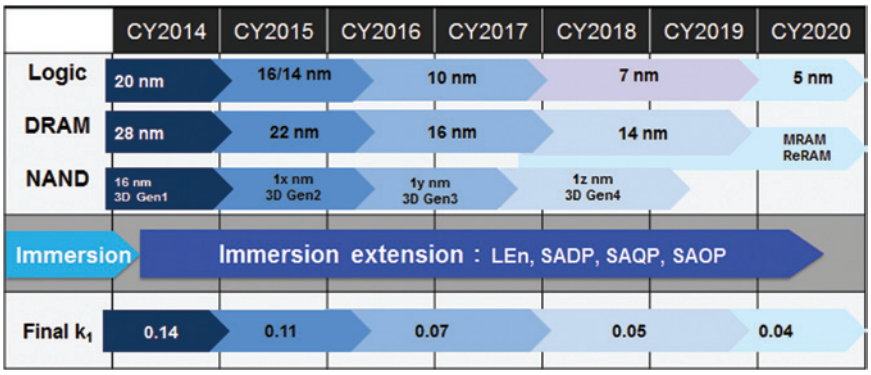

Figure 1: Lithography technology trends form ITRS roadmaps. With the shrinking trend, it is recognized that the ArF immersion lithography can be extended by adopting SADP and SAQP techniques.

(SADP) [4], self-aligned quadruple patterning (SAQP) [5] and even self-aligned octuple patterning (SAOP) [6] techniques.

Due to such extreme low k_1 factor, the accuracy requirements for lithography tools are becoming more and more challenging. In addition, many applications for MPU, memory manufacturers and foundries have different requirements that add to the complexity. In order to meet such severe and wide-ranging requirements, we have developed an ArF immersion scanner that controls a wide variety of parameters contributing to lithography patterning.

2 Illumination pupilgram control

Source mask optimization [7] (SMO) is one of the techniques used to expand lithography margin (dose latitude, depth of focus [DoF]) for below the 28-nm-node generation and beyond. Source shape and mask pattern are iteratively optimized using computational lithography to obtain required litho margin for selected design patterns. This is one way to reduce k_1 factor close of the optical theoretical limit. SMO is widely used for critical layers in ArF immersion lithography.

2.1 SMO and intelligent illuminator unit (IIU)

An example of the effect of SMO [8] is shown in Figure 2. In this figure, we show logic cell pattern for SMO optimization, the SMO illumination source intensity distribution (intensity of 0–1) at the pupil conjugate plane and the expected common process window (exposure latitude [EL] and DoF). We see that the SMO yields ±10% pattern size error from the design intended for pattern #1 when compared with the process window with conventional technique, optical proximity correction (OPC) with a parametric source. We confirm about 30% wider process window for the SMO condition than the conventional OPC technique.

SMO generally requires an intensity distribution that is a complex freeform with intensity located close to the edge of the pupil, because the optimization is for specific patterns, including high spatial frequency components. In order to realize the expected imaging performance of SMO, the exposure tool needs to generate the illumination pupilgram accurately. To do this, a freeform illumination unit called IIU [9] was developed by Nikon. The IIU has a large number of 'degree of pupilgram freedom' (DPF) and allows us to generate the target pupilgram accurately. Conceptually, the DPF is defined below.

$$\text{DPF} = (\text{Gray scale level}) \times (\text{Total number of grid in the pupil})$$

The conceptual diagram of DPF is shown in Figure 3. It can be treated as the number of bricks used to generate pupilgram, in which intensity is defined by the height of piled up bricks in the pupil. To generate target pupilgrams, the IIU calculates how many bricks are needed to be piled up at each position of pupil and sets the bricks in the proper position in the pupil. In IIU, we can use roughly 100 000 degrees of pupilgram freedom. Figure 4 shows the actual measurement results of pupilgrams generated by IIU.

In addition to initial pupilgram generation, the IIU is also used for pupilgram modulation for imaging characteristic tuning such as optical proximity effect (OPE) matching. OPE is usually defined as exposed resist pattern size (critical dimension [CD]) through pattern pitch. Since the mask design is performed based on specific OPE behavior, the exposure tool for the mask needs to have close OPE

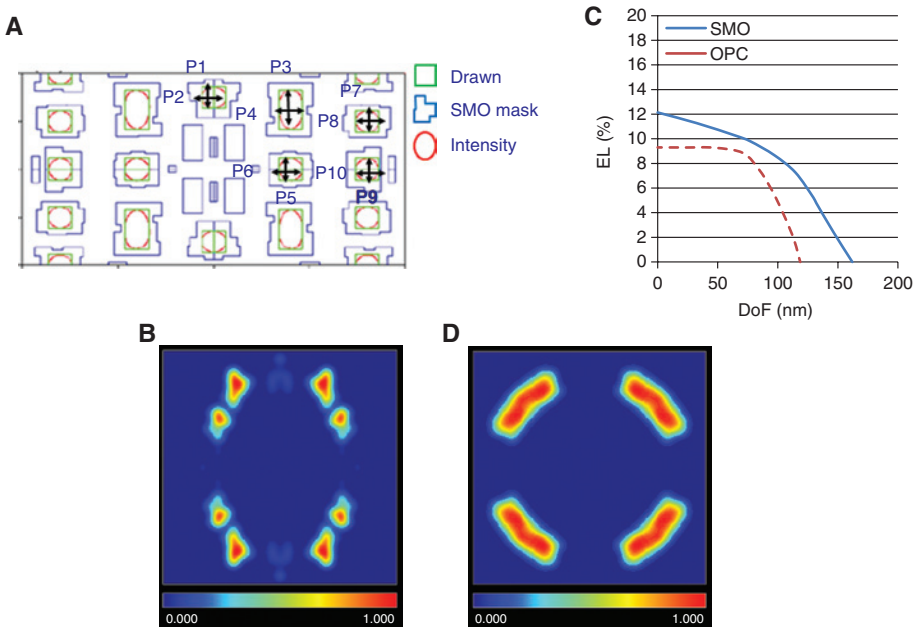

Figure 2: SMO example for logic cell patterns. Design intent pattern (drawn in green) SMO mask pattern in blue, and intensity threshold in red are shown in (A). P1–P9 are gauges for optimization targets. SMO illumination source intensity distribution (intensity of 0–1) in (B). Expected common process window (EL and DoF) shown in blue line in (C) comparing with process window with conventional technique, which is OPC with parametric source shown in (D).

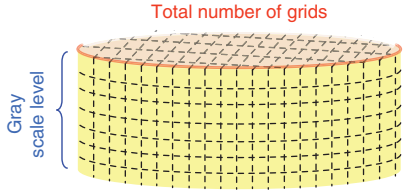

Figure 3: Schematic diagram of definition of DPF.

characteristics to the design assumption. In some cases, the target OPEs are exposure results of the reference exposure tool. In this case, the OPE should match the reference tool.

In the OPE matching procedure, the large number of DPF also helps the user to have accurate pupilgram tuning for reducing OPE matching residual errors. Figure 5 indicates pupilgram modulation accuracy comparison by simulation between different numbers of DPF from 4000 to 100 000. In this example, we assume SMO pupilgram for NAND flash key pattern and Zernike intensity modulation of Z4 (2nd order of pupil coordinates). Zernike intensity modulation is defined as the intensity filter of pupil using Zernike functions. For details, please refer to the appendix at the end of this paper.

As shown in this example, the higher number of PDF shows better representation of the modulated pupilgrams and enables smaller OPE matching residuals than pupilgram modulation with lower number of DPF (see Figure 6). Figure 6 shows dense pattern (1:1 line and space) CD through pitch behavior difference from expectation with the new target pupilgram in Figure 5.

2.2 Pupilgram modulation optimization for OPE matching

In the actual OPE matching procedure tool, software called 'OPE Master' is used for pupilgram optimization [10]. OPE

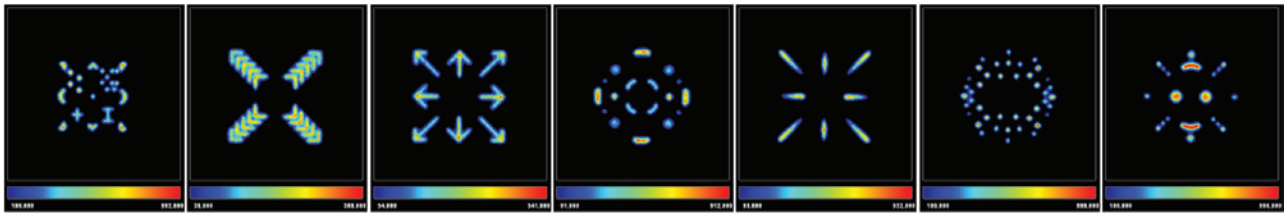

Figure 4: Freeform pupilgrams generated by IIU on ArF immersion exposure tool.

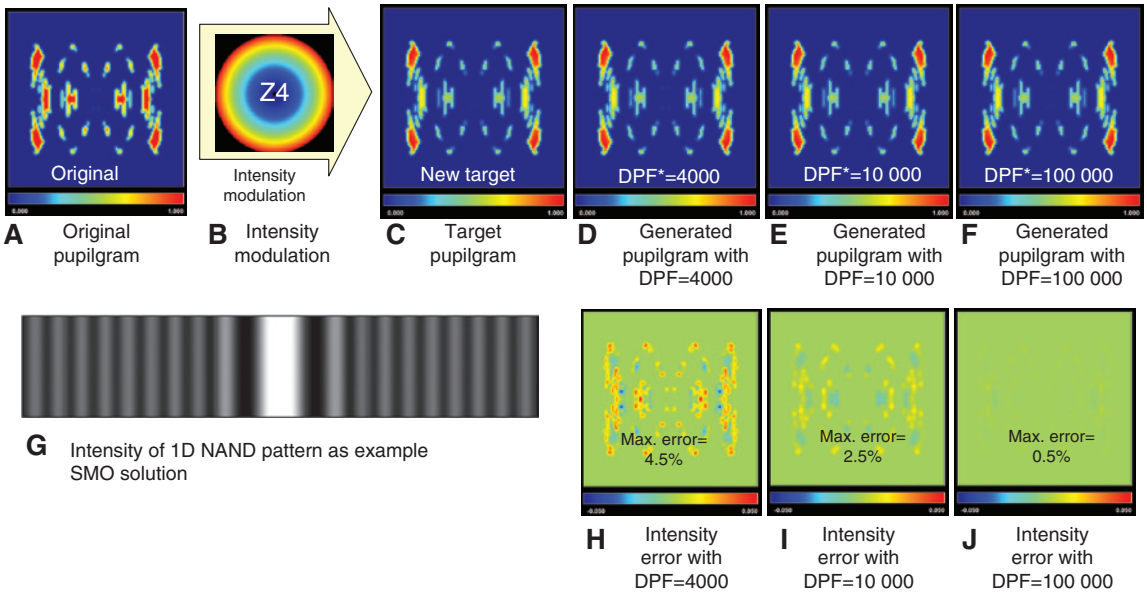

Figure 5: Pupilgram modulation capability comparison between different numbers of DPF (A) original pupilgram. (B) Intensity modulation. (C) Target pupilgram. (D) Generated pupilgram with DPF=4000. (E) Generated pupilgram with DPF=10 000. (F) Generated pupilgram with DPF=100 000. (G) Intensity of 1D NAND pattern as example SMO solution. (H) Intensity error with DPF=4000. (I) Intensity error with DPF=10 000. (J) Intensity error with DPF=100 000.

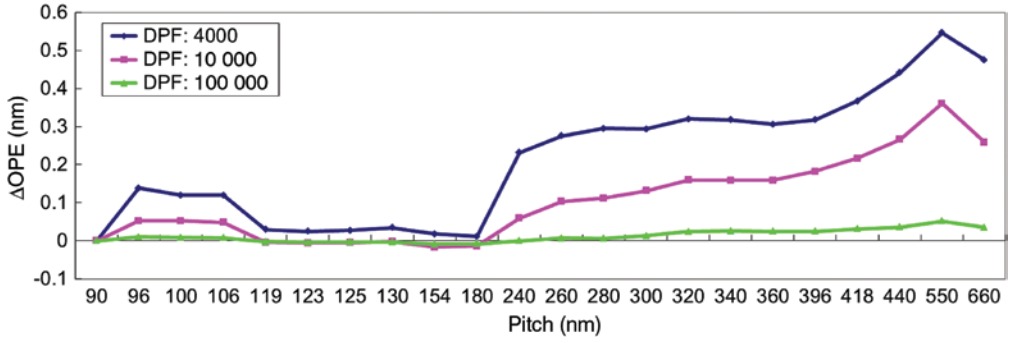

Figure 6: Difference of OPE change from target modulation pupilgram shown in Figure 5 for different numbers of DPF by imaging simulations.

Master can optimize illumination pupilgrams based on pupilgram intensity modulation, pupilgram distortion modulations, etc. The detail of modulations is explained in the appendix. The overall procedure of OPE matching is shown in Figure 7. The OPE matching procedure starts with a test exposure of OPE evaluation with the matching tool. Then, pupilgrams and other optical parameters are optimized by the OPE Master to get similar OPE characteristic as the reference tool. In the optimization, OPE is predicted by imaging simulation using current scanner information such as measured pupilgram, scanner aberration, etc. After the optimization, optimized pupilgram is set on the scanner.

3 Thermal aberration control

In current imaging optics for ArF immersion exposure tool, there are a variety of movable optical elements and adaptive optics, as shown in Figure 8, depicting a current 1.35 NA catadioptric lens. All 3rd order aberrations, primary 5th order aberrations and further higher-order aberration can be modulated electrically. Even field curvature (Petzval field curvature) can be adjusted with reticle bending functionality. As for non-field-dependent component, such as Z5, Z6, etc., a deformable mirror at pupil plane is used to adjust with minimum side effect for field-dependent aberration component.

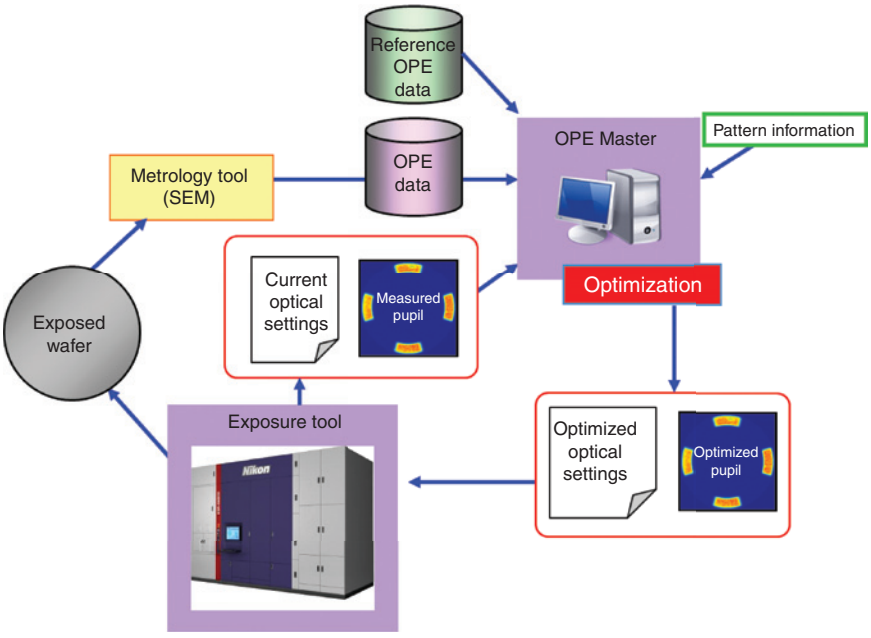

Figure 7: Overall procedure of OPE matching the reference tool.

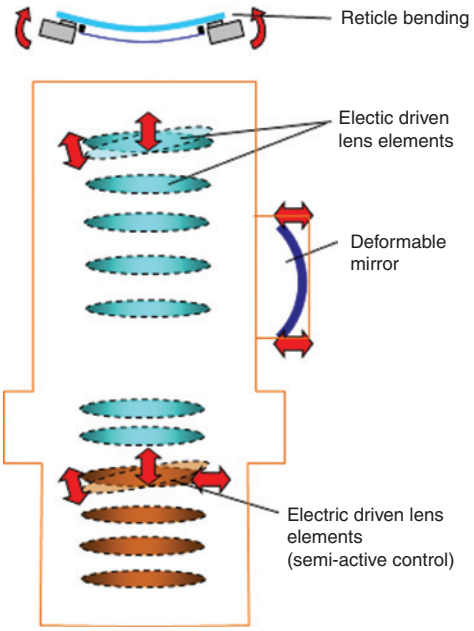

Figure 8: Lens aberration control scheme in 1.35 NA ArF immersion catadioptric lens.

Aberration control system in the imaging optics is called lens controller (LC). The LC is used for lens adjustment, pattern and illumination specific aberration customization and thermal aberration compensation. In order to adjust distortion, the LC is dynamically controlled during scanning exposure. To do this, the position and surface figure of optical elements are controlled in subnanometer level of accuracy dynamically.

In this section, we discuss how to use the LC to compensate thermally induced lens aberration. This is important because, as mentioned above, due to reduction of the k_1 factor, intensity distribution for the most advanced generation of patterning tends to be localized at the edge of pupil. Furthermore, very high productivity such as 200–250 wafers/h exposure requirements makes a very high heat load in the projection lens. Therefore, thermal aberration control is a challenging item for the current exposure tool. In addition, the increase of a variety of layers of the semiconductor manufacturing allows very limited time of LC control parameter adjustment in order to maximize uptime of the exposure tool.

3.1 Lens heat test procedure

Controllers for lens thermal aberrations are not conceptually difficult but do require accurate control parameters describing the lens behavior. Unfortunately, these parameters can depend on the heating pattern induced by the mask projection. Conventionally, thermal aberration control parameters are decided based on the result of dummy exposure tests with reticle (mask) with layer-specific illumination conditions, because the thermal aberration behavior depends on the heat load condition, which is defined by illumination source shape, mask diffraction, exposure field size and power of exposure light. In this heat test, the LC is turned off to see the intrinsic behavior of the thermal aberration. In Figure 9, typical

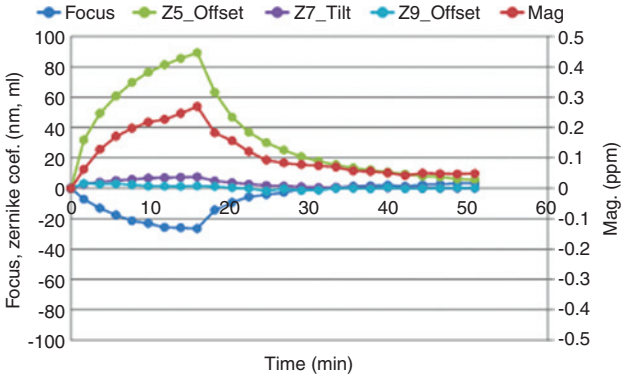

Figure 9: Typical thermal aberration behavior with dipole illumination condition.

thermal aberration behavior in the heat test is shown. The first one-third of the elapsed time shows a heating term during exposure, while the latter two-third shows a cooling term. There are a large amount of focus drift in nm, Zernike Z5 offset (low-order uniform astigmatism) in milli lambda (wavelength is 193 nm) and magnification change in ppm during heating and cooling. From this result, each component of thermal aberration is fit to the thermal aberration model using saturation values for multiple time constants as variable parameter. The saturation values are set as LC parameters to compensate the thermal aberration.

3.2 Computational LC parameter setting and automatic calibration

The heat test is accurate but time consuming. Due to increased productivity requirements, LC parameter setting without the heat test is needed. To meet the requirement, we use offline computational prediction/optimization of the thermal aberration and an automatic calibration and automatic parameter update scheme on the exposure tool [11]. This method requires only limited exposure tool time and can set the LC parameter automatically in the production exposure lot. In order to predict thermal aberration and optimize the LC parameter, software named 'Lens Master' is used. Lens Master predicts the thermal aberration from the mask diffraction pattern, pupilgram shape and field size information. Then, Lens Master optimizes and sets the LC parameter on the exposure tool. This process does not require exposure tool time. As a result, residual thermal aberration in the product exposure can be reduced. In the beginning lot of production, one may observe some remaining error. To correct this error, we use high-speed phase measurement interferometer (PMI) for interval calibration during the beginning lot. By using this method, on-product learning with minimal throughput loss can be achieved. Of course, the following lot can be exposed with high throughput by feed-forward lens control. Lens Master and high-speed PMI enables quick set up of LC parameter for product exposure. Figure 10 shows the validation of this scheme.

4 Critical dimention uniformity (CDU) control

Along with shrinkage of the final pattern size in the roadmap in Figure 1, the required lithography pattern size error across the wafer and across the chip is being reduced. The pattern size uniformity is usually called CDU.

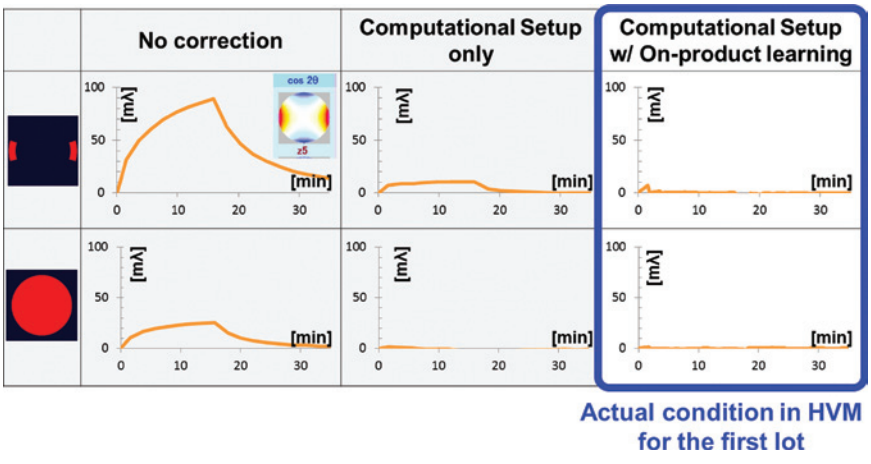

Figure 10: Validation result of the combination on computational setup and on-product calibration/learning.

4.1 CDU error analysis

Figure 11 shows a CDU error analysis in a typical lithography process [12]. The error sources are separated into four main categories: exposure tool, reticle, coater/developer and photo resist material. For the exposure tool, dose and focus deviations are the main causes of CDU degradation. In general, the residual errors for dose and focus after tool setup are <0.1% and 15 nm (3-sigma) during single wafer exposure, and these errors correspond to <0.1 nm CD errors, respectively. Although these CD errors are not negligible, they are not dominant factors from the point of total CDU within a wafer. On the other hand, the reticle has two error sources that include reticle bending and writing error. The bending leads to a defocus distribution within an exposure field. Photo resist thickness error, especially on the wafer edge, and process unit uniformities (post exposure bake [PEB] and developing units) are the main sources of coater/developer-induced effects. Post exposure delay (PED) impacts not only on the average CD value but also on the CDU. These error factors all have a significant influence on CDU. Fortunately, however, they are relatively stable and can be corrected for via precise dose and focus adjustment functions on the exposure tool. This is particularly true in the case of the reticle components, where CD error is repeated field by field and may have a complex distribution that requires high-order correction. In order to decide the offset control of dose and focus, software named CDU Master is used. All software and the exposure tool outlined in this paper were developed by Nikon Corporation, Tokyo, Japan.

4.2 CDU compensation by focus and dose control of exposure tool

CDU Master [12] can be easily utilized to achieve enhanced CDU for finer-pitch CDs patterned with exposure tools. Figure 12 shows a CD correction flow using CDU Master. The exposed wafer is measured by a CD metrology tool, for example, a scatterometry or a CD-SEM system. Then, dose and focus errors are calculated by analysis software. From the calculated dose and focus offset maps, CDU Master generates a subrecipe including high-order optimum dose and focus correction values for each exposure field. Spatial orders of correctable components in field (X, Y) are listed in Table 1 for dose and Table 2 for focus. The optimum value is calculated according to tolerances/limits of the specific exposure tool.

Figure 13 is an example of CDU optimization for 1:1 line/space features in an actual product of lithography. The upper plots show across-wafer CDU, and the bottom plots show intra-field CDU. The left and right show CDU before and after optimization, respectively. About 35–40% CDU improvement can be achieved in both across wafer and intra-field.

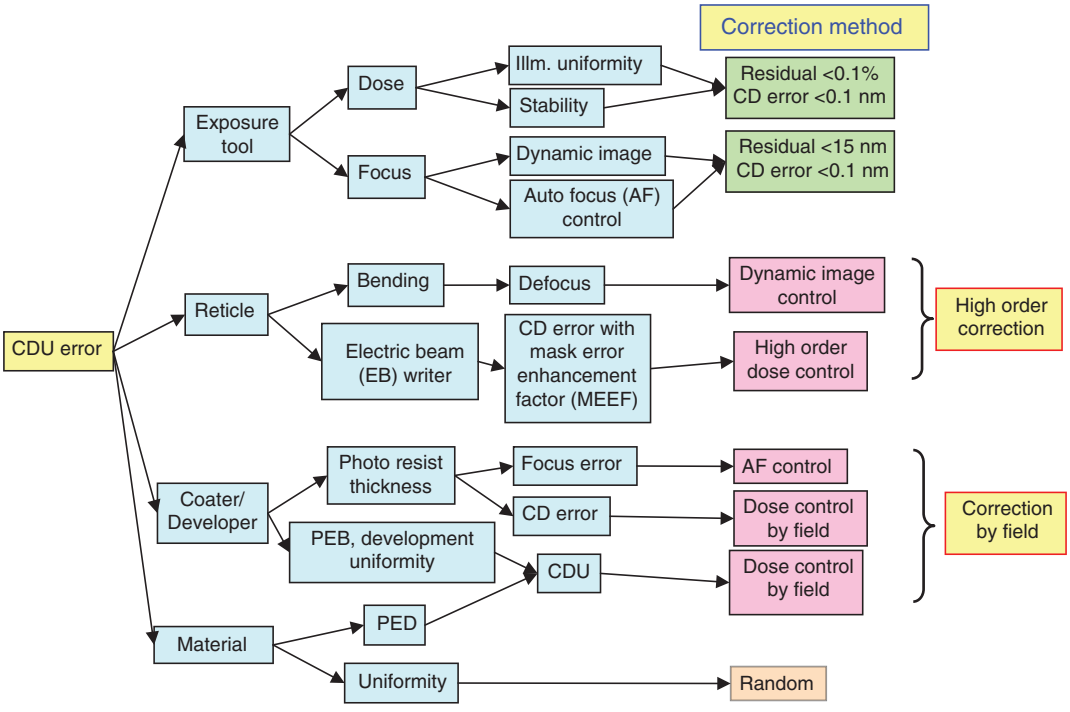

Figure 11: CDU error source analysis.

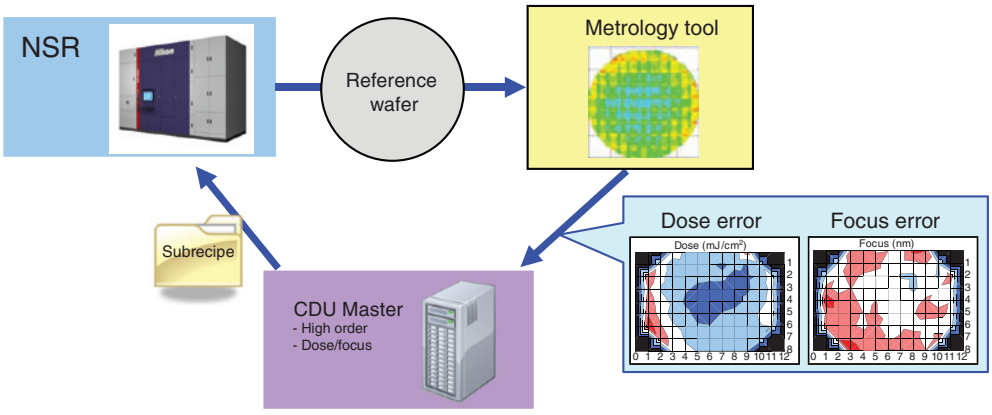

Figure 12: CDU correction flow using CDU Master.

Table 1: Dose correction spatial order for field common and field by field.

Polynomial calculation condition				Y			
				Off	0	1	2~6
		Field common		Yes	Yes	Yes	Yes
			Field by field	Yes	Yes	Yes	-
X	Off	Yes	Yes	Dose, Y, X			
X	1	Yes	Yes				
X	2~6	Yes	-				

Table 2: Focus correction spatial order for field common and field by field.

Polynomial calculation condition				Z(Y)			
				Off	0	1	2~9
		Field common		Yes	Yes	Yes	Yes
			Field by field	Yes	Yes	Yes	Yes
Tilt-X(Y)	Off	Yes	Yes	Z, Y, X	Offset	Offset and tilt	
Tilt-X(Y)	0	Yes	Yes	Tilt-X	Offset and tilt-X	Offset and tilt-X, -Y	
Tilt-X(Y)	1~9	Yes	Yes				

5 Overlay control

Multiple patterning techniques such as LEn, SADP, SAQP, etc., are essential for extremely low k_1 factor lithography. Since overlay accuracy, which is the positioning accuracy between one layer and the following layer, impacts not only overlay but also CDU for the final processed pattern, overlay control is crucial for the multiple patterning.

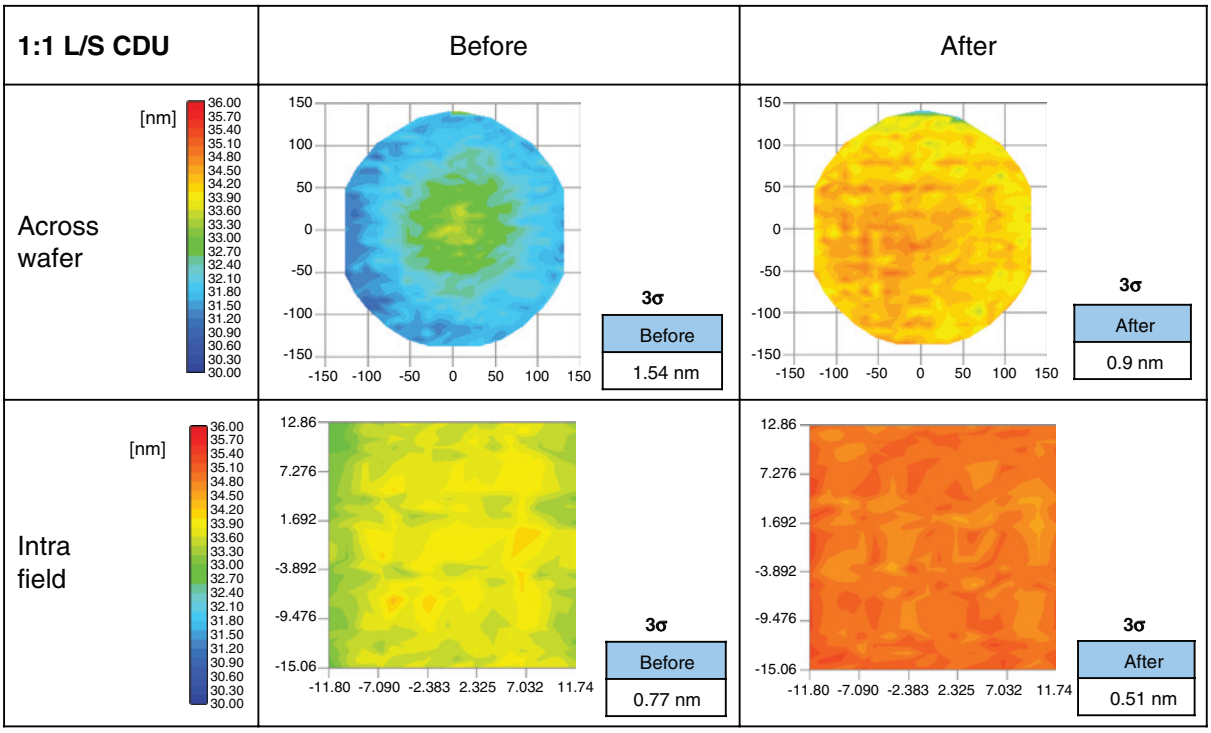

Figure 13: Example of actual product CDU optimization for 1:1 L/S improvement.

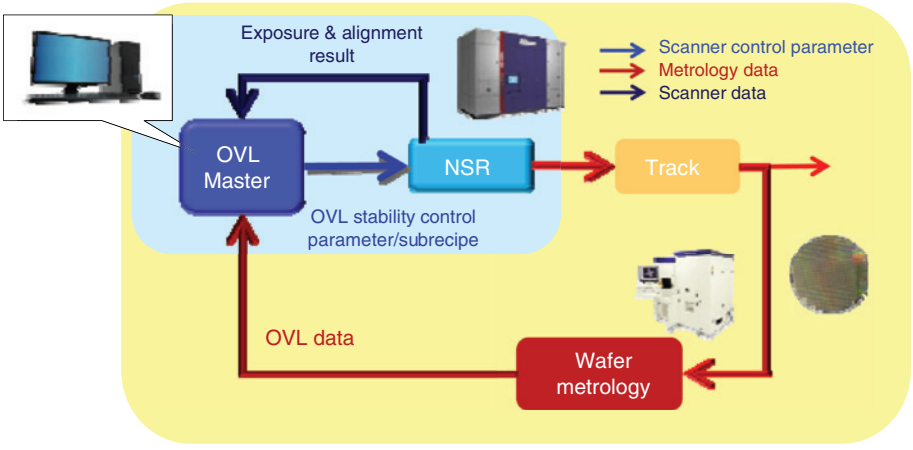

Figure 14: Overall explanation of Overlay Master (OVL Master). Overlay Master calculates optimization parameters based on the metrology result.

5.1 Overlay control by application software

To achieve extremely accurate overlay control, the 4th master application, Overlay Master [13], is prepared. This is application software for overlay optimization, including wafer global and shot local grid. Figure 14 shows the overall flow of Overlay (OVL) Master application. In order to make correction values, a wafer metrology result is needed. The Overlay Master calculates the optimization parameters for scanner overlay control based on the metrology result. Figure 15 shows an example of overlay optimization. This is a one lot mix and match overlay (MMO) result of Nikon NSR S630D #1 vs. S630D #2. S630D with Overlay Master enables <2.3-nm overlay performance. In this optimization, shot-by-shot grid and field correction are included. For grid and field, up to 5th

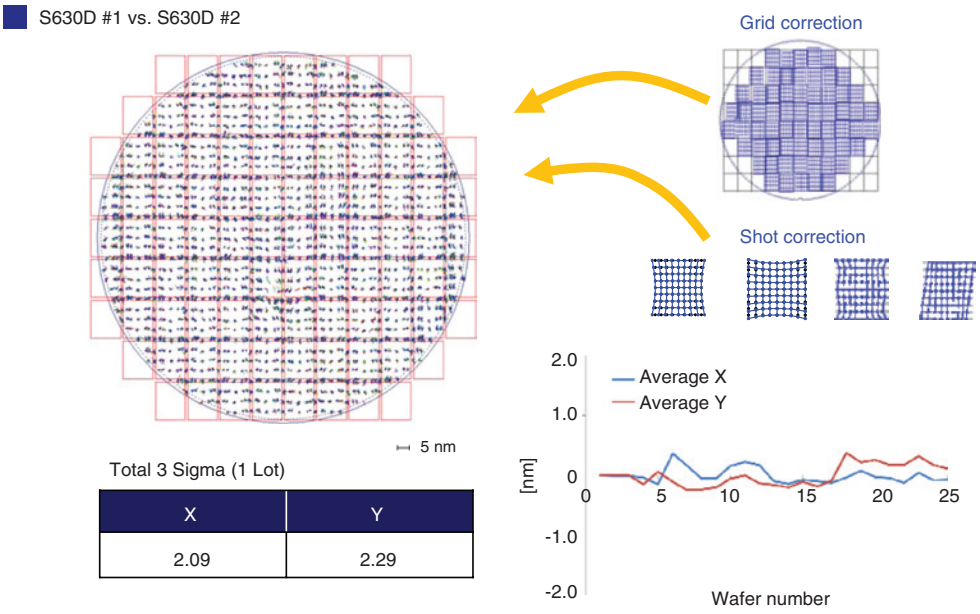

Figure 15: One lot MMO result of S630D #1 vs. S630D #2 in which shot-by-shot grid and field correction are included.

and 3rd order of X, Y coordinates can be corrected, respectively, for function-based control. We can also use map-based compensation for shot-by-shot grid.

6 Summary

ArF immersion with multiple patterning is the main lithography technique even for the 10-nm node generations of semiconductor device and beyond. In these generations, extremely high imaging performance is required of exposure tool in actual production of device due to the extremely low k_1 factor. In order to achieve the requirement, various scanner parameters need to be controlled with feedback or feed-forward loop precisely with limited time of exposure tool usage. We have introduced various technique and application software for the precise exposure tool parameter control: the IIU, OPE Master, adaptive LC, Lens Master, CDU Master and Overlay Master. We confirmed the excellent performance in illumination control, lens control, CDU control and overlay control of exposure tool in conjunction with application software (Masters). Thanks to these Masters, we can use the exposure tool effectively in terms of performance and productivity.

For further generation such as 7 nm, these applications need to be more accurate and predictive. To do this simulation, the performance of each 'Master' should be more physical model than empirical model without sacrificing calculation time. This is for further enhancement of use of ArF immersion tools as even EUV tools become practical for the most critical layers.

Acknowledgments: The author would like to thank Junji Ikeda, Hirotaka Kono, Takayuki Funatsu and Tsuyoshi Toki of Nikon Corporation for helpful discussions and data supply.

Appendix

Pupilgram modulation model

Though the model was originally proposed for pupilgram error analysis, it can be used for freeform pupilgram adjustment. In the model, pupilgram modulation can be expressed by linear combinations of Zernike intensity modulation functions and Zernike distortion modulation functions. These functions are orthogonal and can be expressed by a combination of Zernike polynomials. Some of these polynomials are graphically described in Figure 16. These polynomials are suitable for a Zernike linear combination analysis method to predict the OPE response to changes in the pupilgram. By using this model, we can optimize the intensity distribution of the pupil to minimize the OPE error relatively gently comparing with grid-based optimizations and therefore retaining the pupilgram's original SMO solution characteristics.

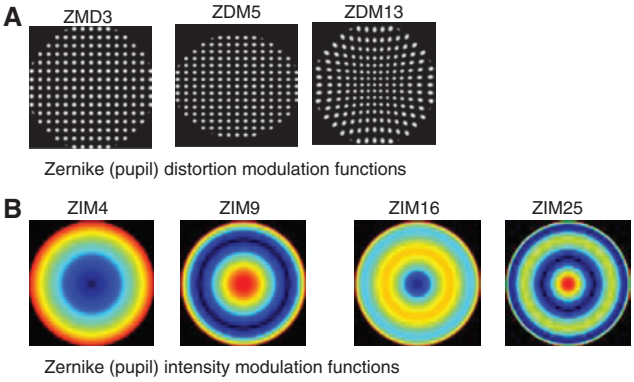

Figure 16: Graphical example of Zernike distortion modulation functions and Zernike intensity modulation functions. (A) Zernike (pupil) distortion modulation functions. (B) Zernike (pupil) intensity modulation functions.

Table 3: Up to 9th order pupil distortion functions.

Number	Pupil distortion function
Dist. 1	$(D_{1x}, D_{1y})=(Z1, 0)$
Dist. 2	$(D_{2x}, D_{2y})=(0, Z1)$
Dist. 3	$(D_{3x}, D_{3y})=(Z2, Z3)$
Dist. 4	$(D_{4x}, D_{4y})=(Z2, -Z3)$
Dist. 5	$(D_{5x}, D_{5y})=(Z3, Z2)$
Dist. 6	$(D_{6x}, D_{6y})=(Z4, 0)$
Dist. 7	$(D_{7x}, D_{7y})=(0, Z4)$
Dist. 8	$(D_{8x}, D_{8y})=(Z5, Z6)$
Dist. 9	$(D_{9x}, D_{9y})=(Z6, -Z5)$
Dist. 10	$(D_{10x}, D_{10y})=(Z5, -Z6)$
Dist. 11	$(D_{11x}, D_{11y})=(Z6, Z5)$
Dist. 12	$(D_{12x}, D_{12y})=(Z7, Z8)$
Dist. 13	$(D_{13x}, D_{13y})=(Z7, -Z8)$
Dist. 14	$(D_{14x}, D_{14y})=(Z8, Z7)$
Dist. 15	$(D_{15x}, D_{15y})=(Z10, Z11)$
Dist. 16	$(D_{16x}, D_{16y})=(Z11, -Z10)$
Dist. 17	$(D_{17x}, D_{17y})=(Z10, -Z11)$
Dist. 18	$(D_{18x}, D_{18y})=(Z11, Z10)$
Dist. 19	$(D_{19x}, D_{19y})=(Z9, 0)$
Dist. 20	$(D_{20x}, D_{20y})=(0, Z9)$
Dist. 21	$(D_{21x}, D_{21y})=(Z12, Z13)$
Dist. 22	$(D_{22x}, D_{22y})=(Z13, -Z12)$
Dist. 23	$(D_{23x}, D_{23y})=(Z12, -Z13)$
Dist. 24	$(D_{24x}, D_{24y})=(Z13, Z12)$
Dist. 25	$(D_{25x}, D_{25y})=(Z17, Z18)$
Dist. 26	$(D_{26x}, D_{26y})=(Z18, -Z17)$
Dist. 27	$(D_{27x}, D_{27y})=(Z17, -Z18)$
Dist. 28	$(D_{28x}, D_{28y})=(Z18, Z17)$
Dist. 29	$(D_{29x}, D_{29y})=(Z14, Z15)$
Dist. 30	$(D_{30x}, D_{30y})=(Z14, -Z15)$
Dist. 31	$(D_{31x}, D_{31y})=(Z15, Z14)$
Dist. 32	$(D_{32x}, D_{32y})=(Z19, Z20)$
Dist. 33	$(D_{33x}, D_{33y})=(Z20, -Z19)$
Dist. 34	$(D_{34x}, D_{34y})=(Z19, -Z20)$
Dist. 35	$(D_{35x}, D_{35y})=(Z20, Z19)$
Dist. 36	$(D_{36x}, D_{36y})=(Z26, Z27)$
Dist. 37	$(D_{37x}, D_{37y})=(Z27, -Z26)$
Dist. 38	$(D_{38x}, D_{38y})=(Z16, 0)$
Dist. 39	$(D_{39x}, D_{39y})=(0, Z16)$
Dist. 40	$(D_{40x}, D_{40y})=(Z21, Z22)$
Dist. 41	$(D_{41x}, D_{41y})=(Z22, -Z21)$
Dist. 42	$(D_{42x}, D_{42y})=(Z21, -Z22)$
Dist. 43	$(D_{43x}, D_{43y})=(Z22, Z21)$
Dist. 44	$(D_{44x}, D_{44y})=(Z28, Z29)$
Dist. 45	$(D_{45x}, D_{45y})=(Z29, -Z28)$
Dist. 46	$(D_{46x}, D_{46y})=(Z23, Z24)$
Dist. 47	$(D_{47x}, D_{47y})=(Z23, -Z24)$
Dist. 48	$(D_{48x}, D_{48y})=(Z24, Z23)$
Dist. 49	$(D_{49x}, D_{49y})=(Z30, Z31)$
Dist. 50	$(D_{50x}, D_{50y})=(Z31, -Z30)$
Dist. 51	$(D_{51x}, D_{51y})=(Z25, 0)$
Dist. 52	$(D_{52x}, D_{52y})=(0, Z25)$
Dist. 53	$(D_{53x}, D_{53y})=(Z32, Z33)$
Dist. 54	$(D_{54x}, D_{54y})=(Z33, -Z32)$
Dist. 55	$(D_{55x}, D_{55y})=(Z34, Z35)$

We define the modulated pupilgram $I_{modulated}(x, y)$ using the equation below.

$$I_{modulated}(x, y)=T(x, y)[I_{original}(x+D_x(x, y), y+D_y(x, y))\otimes PSF]+C \quad (2)$$

where (x, y) is the pupil coordinate, $I_{original}(x+D_x(x, y), y+D_y(x, y))$ is the original pupilgram intensity distribution, $T(x, y)$ is the intensity modulation term, $D_x(x, y)$ is the distortion function in x, $D_y(x, y)$ is the distortion function in y, PSF is a Gaussian point-spread function in pupil that generates blur and C is a constant to express a background intensity offset.

In our definition of distortion, the pure shape modulations are expressed without any intensity modulations. It only describes a 'remapping' of the coordinate positions in the pupil. This equation also defines the hierarchy of the modulation components. The equation is also used for pupilgram error component analysis, which will be discussed in the last section of this paper.

The total intensity filtering effect can be expressed by a sum of component filtering effects $T_i(x, y)$ as

$$T(x, y)=T_1(x, y)\times T_2(x, y)\times\cdots=\prod_i T_i(x, y), \quad (3)$$

where i is a positive integer.

For intensity modulation, we use Fringe Zernike functions, which are very familiar in the microlithography industry as a means to express wavefront aberrations. However, direct use of Fringe Zernike functions would

not be so useful because Fringe Zernike functions take on negative values, which are not realistic for expressing the intensity filtering distribution. In order to make the intensity filtering description physically meaningful, we would need to use a combination of Fringe Zernike functions as basis functions, but such combinations are no longer mutually orthogonal.

Therefore, we propose to use Fringe Zernike functions applied in exponential as

$$T_m(x, y) \equiv \exp[c_m Z_m(x, y)], \tag{4}$$

where m is a positive integer.

In this case, negative values of the Zernike functions are physically meaningful and, when zero, give no filtering effect over the entire pupil.

Now the intensity filtering (modulation) effect can be expressed as a linear combination of Fringe Zernike functions as basis functions, as shown below.

$$T(x, y) = \exp[c_1 Z_1(x, y)] \times \exp[c_2 Z_2(x, y)] \times \cdots = \exp\left[\sum_m c_m Z_m(x, y)\right] \tag{5}$$

One example of the effect of the Zernike intensity modulation is shown in Figure 3.

As for distortion modulation, we cannot directly use the Fringe Zernike functions since they are not sufficient to describe the two-dimensional distortion functions. We therefore propose to use the orthogonal distortion functions shown in Table 3. These are expressed by simple linear combinations of Fringe Zernike functions. The functions form an orthogonal series. We call these Zernike distortion modulation functions.

$$(D_x(x,y), D_y(x,y)) \equiv \sum d_k (D_{kx}(x,y), D_{ky}(x,y)) \tag{6}$$

References

[1] G. Moore, Electronics 38, 8 (1965).

[2] H. Yaegashi, K. Oyama, A. Hara, S. Natori, S. Yamauchi, et al., 'Proc. SPIE 9051, Advances in Patterning Materials and Processes XXXI', 90510X (March 27, 2014).

[3] J. Finders, M. Dusa, B. Vleeming, H. Megens; B. Hepp, et al., 'Proc. SPIE 6924', 692408 (2008).

[4] W.-Y. Jung, C.-D. Kim, J.-D. Eom, S.-Y. Cho, S.-M. Jeon, et al., 'Proc. SPIE6156', 61561J (2006).

[5] H. Yaehashi, K. Oyama, A. Hara, S. Natori and S. Yamauchi, 'Proc. SPIE8325-11', 83250B-1 (2012).

[6] K. Oyama, S. Yamauchi, S. Natori, A. Hara, M. Yamato and H. Yaegashi, 'MNC2013', 6D-2-3 (2013).

[7] A. E. Rosenbluth, S. Bukofsky, C. Fonseca, M. Hibbs, K. Lai, et al., 'Proc. SPIE. 4346', 486 (2001).

[8] H. Aoyama, Y. Mizuno, N. Hirayanagi, N. Kita, R. Matsui, et al., J. Micro/Nanolith. MEMS MOEMS 13, 1:011005R (2013).

[9] Y. Mizuno, T. Matsuyama, S. Owa, O. Tanitsu, N. Kita, et al., 'Proc. SPIE. 7640', 76401I (2010).

[10] T. Matsuyama, N. Kita, R. Matsui and J. Ikeda, 'Proc. SPIE 8326', 83260K (2012).

[11] T. Funatsu, Y. Uehara, Y. Hikida, A. Hayakawa, S. Ishiyama, et al., 'Proc. SPIE. 9426', 942617 (2015).

[12] T. Fujiwara, T. Toki, D. Tanaka, J. Kosugi, T. Susa, et al., 'Proc. SPIE 7973', 797335 (2011).

[13] H. Kono, K. Masaki, T. Matsuyama, S. Wakamoto, S. Park, et al., 'Proc. SPIE. 9426, Optical Microlithography XXVIII', 942619 (2015).